



# Spatial and temporal control of mitochondrial H<sub>2</sub>O<sub>2</sub> release in intact human cells

Michaela Nicole Hoehne<sup>1</sup>, Lianne J H C Jacobs<sup>1</sup> , Kim Jasmin Lapacz<sup>1</sup> , Gaetano Calabrese<sup>1</sup> ,  
Lena Maria Murschall<sup>1</sup>, Teresa Marker<sup>1</sup>, Harshita Kaul<sup>2,3</sup>, Aleksandra Trifunovic<sup>2,3,4</sup> ,  
Bruce Morgan<sup>5</sup> , Mark Fricker<sup>6</sup> , Vsevolod V Belousov<sup>7,8,9,10</sup> & Jan Riemer<sup>1,2,\*</sup> 

## Abstract

Hydrogen peroxide (H<sub>2</sub>O<sub>2</sub>) has key signaling roles at physiological levels, while causing molecular damage at elevated concentrations. H<sub>2</sub>O<sub>2</sub> production by mitochondria is implicated in regulating processes inside and outside these organelles. However, it remains unclear whether and how mitochondria in intact cells release H<sub>2</sub>O<sub>2</sub>. Here, we employed a genetically encoded high-affinity H<sub>2</sub>O<sub>2</sub> sensor, HyPer7, in mammalian tissue culture cells to investigate different modes of mitochondrial H<sub>2</sub>O<sub>2</sub> release. We found substantial heterogeneity of HyPer7 dynamics between individual cells. We further observed mitochondria-released H<sub>2</sub>O<sub>2</sub> directly at the surface of the organelle and in the bulk cytosol, but not in the nucleus or at the plasma membrane, pointing to steep gradients emanating from mitochondria. Gradient formation is controlled by cytosolic peroxiredoxins, which act redundantly and with a substantial reserve capacity. Dynamic adaptation of cytosolic thioredoxin reductase levels during metabolic changes results in improved H<sub>2</sub>O<sub>2</sub> handling and explains previously observed differences between cell types. Our data suggest that H<sub>2</sub>O<sub>2</sub>-mediated signaling is initiated only in close proximity to mitochondria and under specific metabolic conditions.

**Keywords** hydrogen peroxide release; HyPer7; mitochondria; peroxiredoxin

**Subject Categories** Membranes & Trafficking; Organelles

**DOI** 10.15252/emj.2021109169 | Received 8 July 2021 | Revised 16 January 2022 | Accepted 24 January 2022 | Published online 11 February 2022

**The EMBO Journal (2022) 41: e109169**

## Introduction

Reactive oxygen species (ROS) can be toxic molecules. However, some ROS, such as H<sub>2</sub>O<sub>2</sub> can also function as signaling molecules

(Rhee, 1999; D'Autreaux & Toledano, 2007; Janssen-Heininger *et al*, 2008; Holmstrom & Finkel, 2014; Schieber & Chandel, 2014; Riemer *et al*, 2015; Milev *et al*, 2018; Brand, 2020; Sies & Jones, 2020; Winterbourn, 2020). Studies measuring H<sub>2</sub>O<sub>2</sub> release from isolated mitochondria, as well as extracellular H<sub>2</sub>O<sub>2</sub> in cell culture, have indicated that mitochondria are major sites of cellular H<sub>2</sub>O<sub>2</sub> production (Klimova & Chandel, 2008; Murphy, 2009; Brand, 2010, 2016; Drose & Brandt, 2012; McManus *et al*, 2014; Diebold & Chandel, 2016; Wong *et al*, 2019). Unsurprisingly, elevated mitochondrial H<sub>2</sub>O<sub>2</sub> levels have thus been reported to be important for the initiation of a wide range of physiological and pathological responses. Such responses include apoptosis, autophagy, cellular senescence, and HIF1 $\alpha$  signaling, as well as roles in cell proliferation, migration, differentiation, and cell cycle progression (reviewed in, e.g., Chandel, 2014; Brand, 2020; Sies & Jones, 2020).

The mitochondrial respiratory chain and associated substrate dehydrogenases are the major generators of mitochondrial ROS, with respiratory chain complexes I and III the main sites (Murphy, 2009; Brand, 2010). Complex I and complex III activity is therefore presumably key for mediating the physiological and presumably pathological effects caused by mitochondrial ROS. Prominent examples linking ROS generation at these sites with physiological outcomes include hypoxia signaling, where the induction of complex III-dependent ROS generation through antimycin A treatment impacted upon cytosolic HIF1 $\alpha$  stabilization (Klimova & Chandel, 2008), and ischemic reperfusion injury, where reverse electron flow through complex I and consequent ROS generation underlies the pathologic consequences (Chouchani *et al*, 2016; Martin *et al*, 2019). Complexes I and III release ROS to different sides of the mitochondrial inner membrane (IMM), complex I toward the matrix and complex III mainly toward the intermembrane space (IMS; Han *et al*, 2001; Brand, 2010). It should be noted that release of ROS from complex III to the matrix has also been reported (Muller *et al*,

1 Department for Chemistry, Institute for Biochemistry, Redox Biochemistry, University of Cologne, Cologne, Germany

2 Cologne Excellence Cluster on Cellular Stress Responses in Aging-Associated Diseases (CECAD), University of Cologne, Cologne, Germany

3 Institute for Mitochondrial Diseases and Aging, Medical Faculty, University of Cologne, Cologne, Germany

4 Center for Molecular Medicine, University of Cologne, Cologne, Germany

5 Institute of Biochemistry, Centre for Human and Molecular Biology (ZHMB), Saarland University, Saarbruecken, Germany

6 Department of Plant Sciences, University of Oxford, Oxford, UK

7 Department of Metabolism and Redox Biology, Shemyakin-Ovchinnikov Institute of Bioorganic Chemistry, Moscow, Russia

8 Center for Precision Genome Editing and Genetic Technologies for Biomedicine, Pirogov Russian National Research Medical University, Moscow, Russia

9 Federal Center of Brain Research and Neurotechnologies, FMBA, Moscow, Russia

10 Institute for Cardiovascular Physiology, Georg August University Göttingen, Göttingen, Germany

\*Corresponding author (lead contact). Tel: +49 221 470 7306; E-mail: jan.riemer@uni-koeln.de

2004). This spatial specificity of ROS generation and release has been confirmed by redox proteomics data on isolated mitochondria; when ROS production was induced by inhibitor treatment of complexes I and III, proteins that were oxidatively modified, localized mainly to matrix and IMS, respectively (Bleier *et al*, 2015).

The proximal ROS produced by the mitochondrial respiratory complexes are superoxide anions that are rapidly dismutated to H<sub>2</sub>O<sub>2</sub> and oxygen either by superoxide dismutase 2 (SOD2) in the matrix or SOD1 in the IMS, depending on the site of their generation. H<sub>2</sub>O<sub>2</sub>, but not superoxide, can diffuse relatively slowly across the IMM, while porins/VDACs in the outer membrane (OMM) likely allow for an unimpeded diffusion, for example, into the cytosol. In the case of the IMM, it remains possible that transport might be facilitated by a yet unknown transporter(s) as have been found in other cellular membranes (Calamita *et al*, 2005; Bienert *et al*, 2007; Marchissio *et al*, 2012). Subcellular compartment-specific concentrations of H<sub>2</sub>O<sub>2</sub> are set mainly by rates of production (activities of superoxide generator sites and SODs), removal through the activities of antioxidative enzyme systems (peroxiredoxins, catalases), diffusion of H<sub>2</sub>O<sub>2</sub> into or out of the compartment of interest (for example, mitochondrial H<sub>2</sub>O<sub>2</sub> release to the cytosol), or via reactions with biomolecules like proteins or lipids. Furthermore, site-specific generation of H<sub>2</sub>O<sub>2</sub> combined with the presence of efficient scavenging systems, likely leads to the presence of steep H<sub>2</sub>O<sub>2</sub> gradients even within specific subcellular compartments (Pak *et al*, 2020; Niemeyer *et al*, 2021). Therefore, in order to act as signaling molecule outside mitochondria, mitochondrial H<sub>2</sub>O<sub>2</sub> would have to: (i) be produced in sufficient amounts to avoid being completely scavenged by local antioxidative systems or by side reactions with mitochondrial biomolecules; (ii) would have to navigate the complex morphology of mitochondria in order to reach the cytosol, including crossing one or two membranes; (iii) would have to react preferentially with putative cytosolic target proteins instead of being scavenged by the potent cytosolic H<sub>2</sub>O<sub>2</sub> removal enzymes.

The dynamics of H<sub>2</sub>O<sub>2</sub> inside mitochondria and of mitochondria H<sub>2</sub>O<sub>2</sub> release is poorly understood in mammalian cells. Previous studies have relied on tools including matrix-targeted or untargeted small molecule chemical probes, for example Mito-SOX, or low sensitivity genetically encoded probes, for example, HyPer3 or roGFP2-Orp1. Small molecule chemical probes do not allow high resolution monitoring of extramitochondrial H<sub>2</sub>O<sub>2</sub>, are typically irreversible and thus do not permit monitoring of dynamic H<sub>2</sub>O<sub>2</sub> changes, and can be affected by differential cellular uptake and efflux. Low sensitivity genetically encoded probes only respond to strong exogenous H<sub>2</sub>O<sub>2</sub> treatments or are strongly influenced by redox changes in the glutathione pool, which is normally required for sensor reduction. Finally, H<sub>2</sub>O<sub>2</sub> release has been assessed using isolated mitochondria or measurements of extracellular H<sub>2</sub>O<sub>2</sub> (both as proxies for mitochondrial H<sub>2</sub>O<sub>2</sub> release inside cells; Goncalves *et al*, 2015; Roma *et al*, 2018; Kalinovic *et al*, 2019; Liao *et al*, 2020; Plecita-Hlavata *et al*, 2020). Such measurements on isolated mitochondria necessarily ignore the role of cytosolic redox systems and thus fail to represent the cellular situation. Likewise, measurements outside cells with highly sensitive methods might detect concentrations well below the point of biological activity, but fail to directly report on mitochondrial H<sub>2</sub>O<sub>2</sub> release and the local internal concentrations or gradients. Thus, although mitochondrial H<sub>2</sub>O<sub>2</sub> appears to have important roles in many signaling or pathological phenotypes,

*in situ* evidence for its release from mitochondria in intact cells and its subsequent dynamics in the cytosol remains scarce.

Recently, a highly-sensitive, pH-insensitive H<sub>2</sub>O<sub>2</sub> sensor, HyPer7, was developed, which allows for dynamic measurement of highly localized changes in intracellular H<sub>2</sub>O<sub>2</sub> concentration (Pak *et al*, 2020). Notably, experiments with HyPer7 cast doubt on the release of mitochondrial H<sub>2</sub>O<sub>2</sub> into the cytosol (Pak *et al*, 2020) as no H<sub>2</sub>O<sub>2</sub> release could be detected upon rotenone- or matrix-targeted D-amino acid oxidase-induced mitochondrial H<sub>2</sub>O<sub>2</sub> generation. Only upon simultaneous inhibition of the cytosolic thioredoxin system, was an increase in H<sub>2</sub>O<sub>2</sub> detected in the cytosol.

Here, we employed the HyPer7 sensor to revisit mitochondrial H<sub>2</sub>O<sub>2</sub> release in a number of cell types. We demonstrate that in different settings, mitochondria do indeed release sufficient H<sub>2</sub>O<sub>2</sub> to be detectable at the OMM and in the bulk cytosol. H<sub>2</sub>O<sub>2</sub> release is strictly controlled by the metabolic state of the cell in a janus-faced manner: on the one hand, higher activity of the respiratory chain in cells grown on galactose increases H<sub>2</sub>O<sub>2</sub> generation, on the other hand it also increases the level of cytosolic thioredoxin reductase to facilitate H<sub>2</sub>O<sub>2</sub> removal. Intriguingly, we find that the H<sub>2</sub>O<sub>2</sub> scavenging capacity of the cytosolic peroxiredoxins is limited and regulated by changes in thioredoxin reductase availability. Changes in thioredoxin reductase level underlie the increased cytosolic H<sub>2</sub>O<sub>2</sub> scavenging capacity observed in galactose grown cells and can explain apparent cell-type differences in the amount of mitochondrial H<sub>2</sub>O<sub>2</sub> detected in the cytosol. Our data thus suggest that the cytosolic peroxiredoxins, PRDX1 and PRDX2, have a “reserve capacity” and are present at a level in excess of their requirement for H<sub>2</sub>O<sub>2</sub> scavenging. Our results point to a synchronized adaptation of cytosolic redox systems in response to changing metabolic states that influence mitochondrial H<sub>2</sub>O<sub>2</sub> release, while still allowing direct H<sub>2</sub>O<sub>2</sub> signaling in close proximity to mitochondria.

## Results

### Antimycin A treatment induces cytosolic responses of HyPer7

Little is known about the spatio-temporal organization of mitochondrial H<sub>2</sub>O<sub>2</sub> release or removal in intact human cells. We made use of the genetically encoded fluorescent probe, HyPer7, which allows the real-time monitoring of basal H<sub>2</sub>O<sub>2</sub> levels with unprecedented sensitivity in specific subcellular compartments (Pak *et al*, 2020; Fig 1A), to characterize mitochondrial H<sub>2</sub>O<sub>2</sub> dynamics and release into the cytosol. HyPer7 comprises a circular permuted yellow fluorescent protein (cpYFP) genetically inserted into the OxyR regulatory domain (OxyR-RD) of *Neisseria meningitidis*. The OxyR-RD moiety of the HyPer7 probe responds directly to H<sub>2</sub>O<sub>2</sub> by forming a disulfide bond. This in turn induces a shift in the fluorescence excitation spectrum of cpYFP. While the probe is oxidized by H<sub>2</sub>O<sub>2</sub>, it is predominantly reduced by endogenous thioredoxins (Kritsiligkou *et al*, 2021). HyPer7 oxidation is therefore determined by rapid H<sub>2</sub>O<sub>2</sub>-driven oxidation and slower thioredoxin-driven reduction (Fig 1A; Pak *et al*, 2020). In our experimental setup, the readout of HyPer7 can be presented as ratio of fluorescence emission intensity following excitation at 469 and 390 nm. Such ratiometric measurements are automatically compensated against varying probe concentration (for data acquisition and analysis using a multi-well microscope setup, see Materials and Methods). An increase or decrease in the 469/390 ratio

corresponds to an increased or decreased average probe oxidation, respectively. This was clearly visible when we monitored single cell responses of cytosolic HyPer7 in HEK293 cells to the repeated addition of exogenous H<sub>2</sub>O<sub>2</sub> (Fig 1B). We observed that with H<sub>2</sub>O<sub>2</sub> applied exogenously at a concentration as low as 2 μM, HyPer7 responded by becoming more oxidized, albeit with considerable cell-to-cell heterogeneity. To transparently report on this cell-to-cell heterogeneity that we observed in all our experiments with HyPer7, while still allowing for an easy assessment of the data, we present our data both as an average over many cells (Fig 1A and B, solid black line) and as single cell data (Fig 1A and B, light gray data points). Although HyPer7 is considerably more sensitive than previous H<sub>2</sub>O<sub>2</sub> sensors, including roGFP2-Orp1 and HyPer3, it was still almost completely reduced under steady state conditions as DTT treatment did not cause a further reduction of the fluorescence excitation ratio of the sensor in the cytosol of HEK293 cells (Appendix Fig S1).

To obtain a better overview of subcellular H<sub>2</sub>O<sub>2</sub> dynamics upon induction of mitochondrial H<sub>2</sub>O<sub>2</sub> production, we also targeted HyPer7 to the mitochondrial matrix, IMS, the cytosolic side of the OMM, the plasma membrane (PM), and the nucleus (Fig 1C). We then monitored the HyPer7 responses in HEK293 cells upon treatment with antimycin A, a complex III inhibitor. Antimycin A causes release of superoxide anions (which are rapidly dismutated to H<sub>2</sub>O<sub>2</sub>) toward the IMS side of the IMM as well as likely also increasing superoxide production at complex I. We performed these experiments with cells grown in glucose or galactose (cells were adapted to galactose growth for at least one week) as the carbon source. Compared to glucose, galactose enhances oxidative metabolism and thus might be expected to generate more superoxide anions upon antimycin A treatment (Appendix Fig S2). In the IMS, we observed a small HyPer7 response that was more pronounced in cells grown on galactose than in cells grown on glucose (Fig 1D). Interestingly, matrix-targeted HyPer7 appeared to react even more strongly than its IMS counterpart, likely representing diffusion of H<sub>2</sub>O<sub>2</sub> (or perhydroxyl radicals) over the IMM from the cristae space or partial direct release of ROS from complex III toward the matrix (Fig 1E). Similar to the IMS and matrix, we also observed a stronger response in cells grown on galactose for the OMM and cytosolic HyPer7 probes (Figs 1F and G). Notably, cytosolic HyPer7 reacted only to antimycin A treatment when cells were grown on galactose. However, no HyPer7 response was observed to antimycin A treatment in the nucleus or on the PM, in cells grown on galactose (Fig 1H). We could confirm these findings using the complex I inhibitor rotenone (Appendix Fig S3). Treatment with rotenone resulted in detectable HyPer7 responses in the cytosol if HEK293 cells were grown on galactose. In summary, antimycin A treatment resulted in detectable deflections of HyPer7 at the OMM and in the cytosol, but not in the nucleus or at the plasma membrane, a finding which supports the existence of a steep H<sub>2</sub>O<sub>2</sub> concentration gradient emanating from the mitochondrial surface. HyPer7 responses in cells grown in galactose-containing medium were in general more pronounced, indicating that the H<sub>2</sub>O<sub>2</sub> gradient is modulated by metabolic adaptations (e.g., differences in H<sub>2</sub>O<sub>2</sub> generation).

### Galactose-grown cells present stronger HyPer7 responses after hypoxia-reoxygenation

Given our observation of metabolic state-dependent detection of mitochondrial H<sub>2</sub>O<sub>2</sub> in the cytosol, we asked whether we could

confirm these findings in a more physiologically relevant situation, namely hypoxia-reoxygenation. To this end, we exposed cells to hypoxia for 200 min followed by reoxygenation or to continuous hypoxia. Reoxygenation should increase the generation of H<sub>2</sub>O<sub>2</sub> particularly in mitochondria. During hypoxia, the absolute HyPer7 ratios in all compartments assessed were lower than in normoxic cells, but remained unchanged over an extended period indicating that hypoxia alone did not result in substantial H<sub>2</sub>O<sub>2</sub> generation (Fig 2A–E, compare black line and red line before 200 min). Upon reoxygenation HyPer7 became more oxidized in all compartments assessed, particularly if cells had been grown in galactose-containing medium (Fig 2A–D). In cells maintained constantly in hypoxic conditions, HyPer7 ratios did not change (Fig 2A–E, black line).

### Equal mitochondrial H<sub>2</sub>O<sub>2</sub> generation results in detection of different cytosolic H<sub>2</sub>O<sub>2</sub> amounts upon growth in the presence of different carbon sources

The amount of H<sub>2</sub>O<sub>2</sub> generated by incubation of cells with antimycin A depends on the activity of the respiratory chain. We modulated electron flux through the respiratory chain by providing cells with different carbon sources. However, this also impacts many other cellular processes including the generation of NADPH, for example by modulating flux through the pentose phosphate pathway. To distinguish the effects of increased mitochondrial H<sub>2</sub>O<sub>2</sub> production from general changes in other cellular processes in cells grown on galactose, we turned to a genetically engineered H<sub>2</sub>O<sub>2</sub> producing system using matrix-targeted C-terminally FLAG-tagged D-amino acid oxidase (mtDAO, Fig 3A; Matlashov *et al*, 2014; Pak *et al*, 2020). Using the TRex-FlpIn system, we generated stable cell lines to ensure homogenous expression of mtDAO in all cells. Moreover, we employed a doxycycline-inducible mtDAO expression system to minimize adaptation effects that might result from a continuous expression of this enzyme. After 24 h induction of mtDAO expression and upon subsequent addition of D-alanine, but not L-alanine, mtDAO produced H<sub>2</sub>O<sub>2</sub> in a dose-dependent manner in the mitochondrial matrix (Fig 3B).

We then used this system to monitor HyPer7 responses in different compartments of cells grown on galactose- or glucose-containing medium (Fig 3C). We detected HyPer7 oxidation in all compartments upon addition of 2 mM of D-alanine demonstrating that in this controlled setting H<sub>2</sub>O<sub>2</sub> is produced and released from mitochondria. The HyPer7 response in the matrix was similar between glucose and galactose-grown cells. Interestingly, the response of HyPer7 in the cytosol and the IMS was less pronounced in cells grown on galactose compared to growth on glucose, the opposite trend to that observed with antimycin A or re-oxygenation. Likewise, the response at the OMM was similarly independent of the growth medium, an observation that we currently cannot explain, as it also appears to differ from antimycin A and reoxygenation treatments. In the nucleus and on the PM, the HyPer7 probe only responded at 8 mM of D-alanine (Appendix Fig S4). Collectively, our data indicate that upon production of a defined quantity of H<sub>2</sub>O<sub>2</sub> in the matrix the amount that is detected in the cytosol is reduced in cells grown on galactose compared to cells grown on glucose.

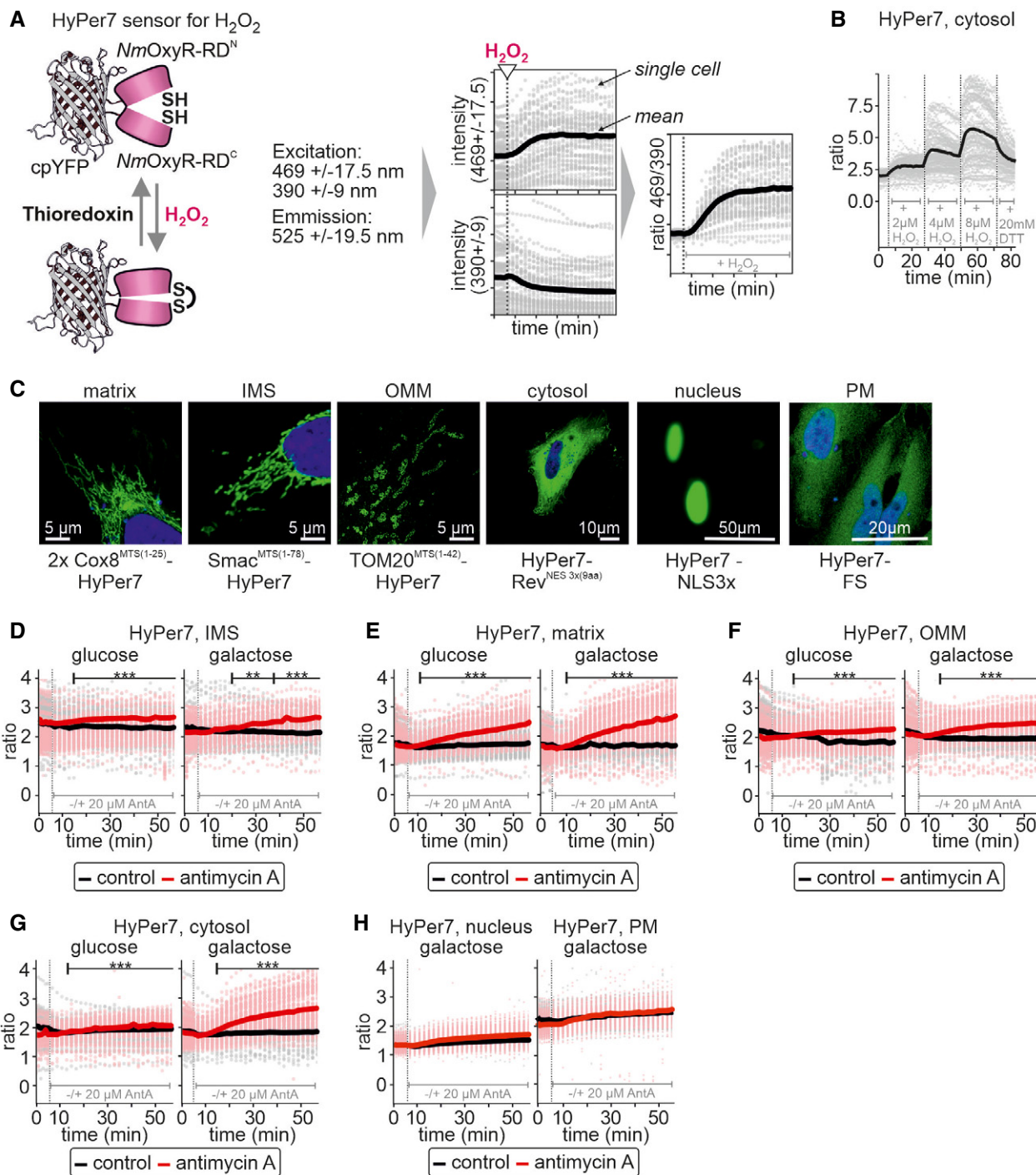


**Figure 1. Antimycin A treatment induces responses of cytosolic HyPer7.**

- A The H<sub>2</sub>O<sub>2</sub> sensing mechanism of the HyPer7 probe and representation of data.
- B The response of cytosolic HyPer7 in HEK293 cells to repeated bolus of exogenous H<sub>2</sub>O<sub>2</sub> at the indicated concentrations. Solid line represents mean, light gray points are ratios measured in individual cells.
- C Confirmation of sensor localization to different cellular compartments. Green, HyPer7; blue, DAPI stain.
- D–H Response of HyPer7 probes targeted to indicated compartments to incubation with antimycin A (a complex III inhibitor, red curve, and data points) or ethanol as control (black line and data points). HEK293 cells were grown either with glucose or galactose as carbon source as indicated. Solid line represents mean, points colored in the lighter version of the respective color are the corresponding ratios measured in individual cells.

Data information: The numbers of cells per experiment for each dataset can be found in Appendix Table S6. As most of the data were not normal distributed, instead of a t-test, a Wilcoxon/Mann–Whitney-U-test was performed and samples were compared in pairs. \*\**P* ≤ 0.01, \*\*\**P* ≤ 0.001.

Source data are available online for this figure.

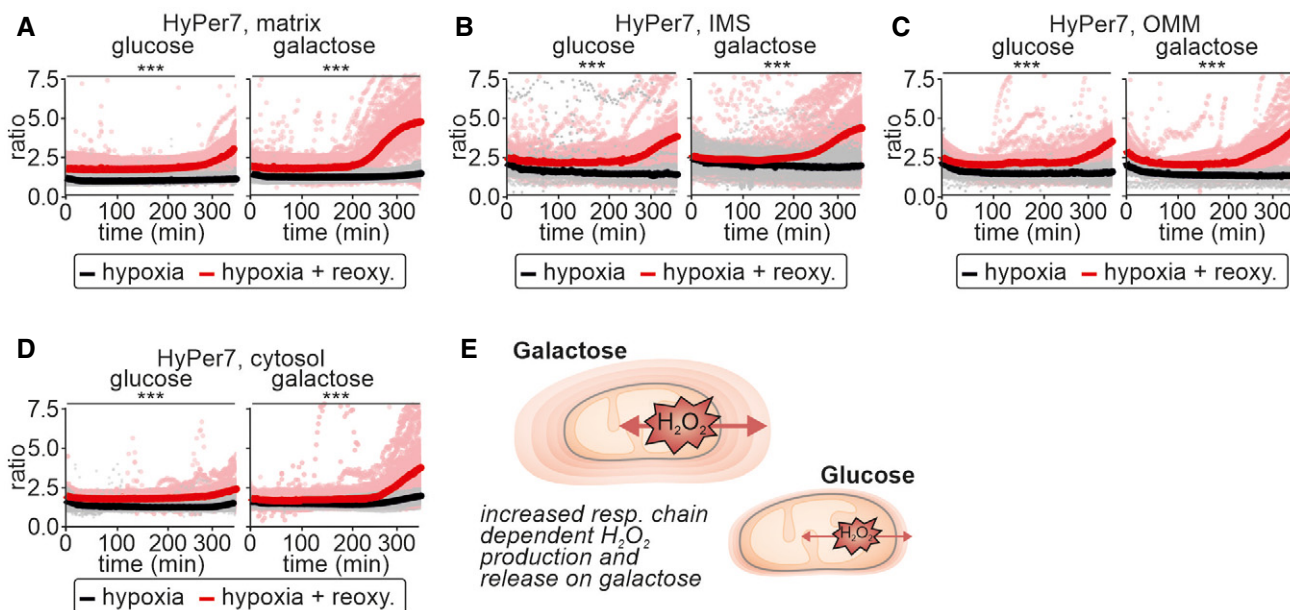


**Figure 2. Galactose-grown cells present with stronger HyPer7 responses upon reoxygenation after hypoxia.**

A–D Response of HyPer7 probes targeted to indicated compartments to reoxygenation after hypoxia (red curve and data points) or to continued hypoxia (black line and data points). HEK293 cells were grown either with glucose or galactose as carbon source. Solid line represents mean, points colored in the lighter version of the respective color are the corresponding ratios measured in individual cells.

E Model. Cells grown on galactose-containing medium exhibit increased production of H<sub>2</sub>O<sub>2</sub> and thus also increased detection of cytosolic H<sub>2</sub>O<sub>2</sub> indicating H<sub>2</sub>O<sub>2</sub> gradients of different steepness around mitochondria.

Data information: The numbers of cells per experiment for each dataset can be found in Appendix Table S6. As most of the data were not normal distributed, instead of a t-test, a Wilcoxon/Mann–Whitney-U-test was performed and samples were compared in pairs. \*\*\*P ≤ 0.001.

Source data are available online for this figure.

### Growth in the presence of different carbon sources impacts compartmental H<sub>2</sub>O<sub>2</sub> handling

With our different treatment regimes, we obtained seemingly contradicting results: antimycin A treatment and reoxygenation after hypoxia induced a more prominent oxidation of cytosolic HyPer7 on galactose-grown compared to glucose-grown cells, while for mtDAO-induced H<sub>2</sub>O<sub>2</sub> generation we observed the opposite. One explanation for these findings might be prior adaptation processes on galactose that strengthen cellular antioxidative systems and therefore H<sub>2</sub>O<sub>2</sub> scavenging capacity. This might make biological sense as a mechanism to counteract the increased amounts of H<sub>2</sub>O<sub>2</sub> produced as a consequence of increased flux through the respiratory chain. Antimycin A treatment would still lead to high H<sub>2</sub>O<sub>2</sub> production that exceeds the capacity of the antioxidative systems, hence the stronger oxidation of HyPer7 with antimycin A on galactose. Conversely, the mtDAO system produces similar amounts of H<sub>2</sub>O<sub>2</sub> on both glucose and galactose, but the more efficient antioxidative systems on galactose would attenuate the impact of its release. To further test this hypothesis, we exposed HEK293 cells to bolus treatments with exogenous H<sub>2</sub>O<sub>2</sub>. Indeed, in all compartments, the HyPer7 response was attenuated in cells grown on galactose compared to glucose (Fig 4A).

Thus, in HEK293 cells, we demonstrate that different modes of mitochondrial H<sub>2</sub>O<sub>2</sub> production (e.g., antimycin A, mtDAO) result in release of H<sub>2</sub>O<sub>2</sub> from mitochondria. However, growth of cells on a

carbon source that induces increased electron flux through the respiratory chain (galactose) also appears to upregulate anti-oxidant pathway(s) allowing cells to handle H<sub>2</sub>O<sub>2</sub> more efficiently, and thus attenuates the consequences of mitochondrial H<sub>2</sub>O<sub>2</sub> release (Fig 4B).

### Increased activity of the cytosolic thioredoxin system reduces the impact of mitochondrial H<sub>2</sub>O<sub>2</sub> release during increased activity of the respiratory chain

We next sought to determine the specific protein changes that are induced by cell growth on galactose relative to glucose by performing quantitative proteomics of HEK293 (Fig 5A, Dataset EV1). Expectedly, the amounts of many proteins differed between the two conditions; however, we only observed a significant difference in one protein that qualifies as an antioxidative enzyme. This was the cytosolic thioredoxin reductase 1, TXNRD1, which was increased about 2- to 2.5-fold in cells grown on galactose compared to glucose-grown cells. Notably, the levels of the cytosolic peroxiredoxins remained unchanged. We confirmed this result by immunoblotting against selected redox proteins (Fig 5B).

We then tested the involvement of the thioredoxin system in regulating H<sub>2</sub>O<sub>2</sub> dynamics. To this end, we inhibited thioredoxin reductase using auranofin (Fig 5C). Auranofin treatment strongly increased oxidation of the cytosolic HyPer7 sensor during mtDAO-

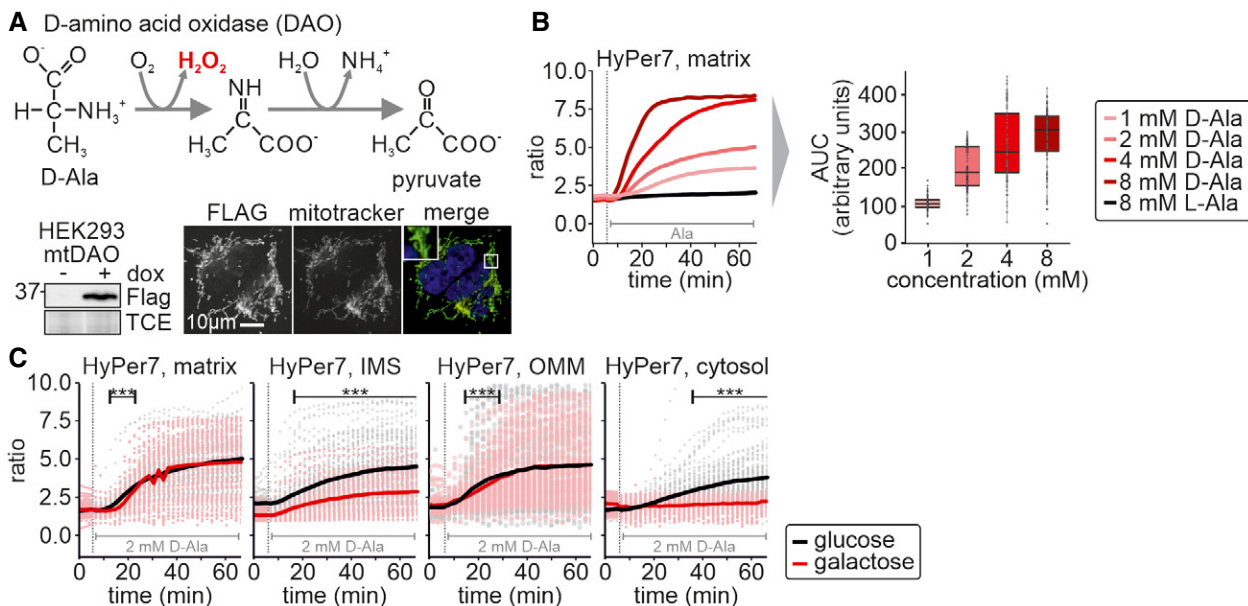


**Figure 3. Equal mitochondrial H<sub>2</sub>O<sub>2</sub> generation results in detection of different cytosolic H<sub>2</sub>O<sub>2</sub> amounts upon growth in the presence of different carbon sources.**

- A Mechanism of D-amino acid oxidase (DAO) in the production of H<sub>2</sub>O<sub>2</sub>. Cell lines stably and inducibly expressing a mitochondrial matrix version of DAO (mtDAO) were generated and tested by immunoblot and immunofluorescence.
- B Titration of D-alanine (D-Ala) in mtDAO-containing cells and monitoring by matrix HyPer7 (cell generated with the Flp-In T-REX-system). Solid line represents average of multiple measure cells. For area under the curve (AUC) analyses, means of control curves were subtracted from means of D-Ala-treated cells. In the box plot, the central band is the median. The lower and upper hinges correspond to the first and third quartiles. The upper whisker extends from the hinge to the largest value no further than 1.5 times the inter-quartile range, whereas the lower whisker extends from the hinge to the smallest value no further than 1.5 times the inter-quartile range. The numbers of cells per experiment for each dataset can be found in Appendix Table S6.
- C Response of HyPer7 probes targeted to indicated compartments to treatment of mtDAO-expressing HEK293 cells with 2 mM D-Ala (cells generated with the Flp-In T-REX-system). HEK293 cells were grown either with glucose (black curve and data points) or galactose (red curve and data points) as carbon source. Solid line represents average, points colored in the lighter version of the respective color are the corresponding ratios measured in individual cells.

Data information: The numbers of cells per experiment for each dataset can be found in Appendix Table S6. As most of the data were not normally distributed, instead of a t-test, a Wilcoxon/Mann-Whitney-U-test was performed and samples were compared in pairs. \*\*\*P ≤ 0.001. Source data are available online for this figure.

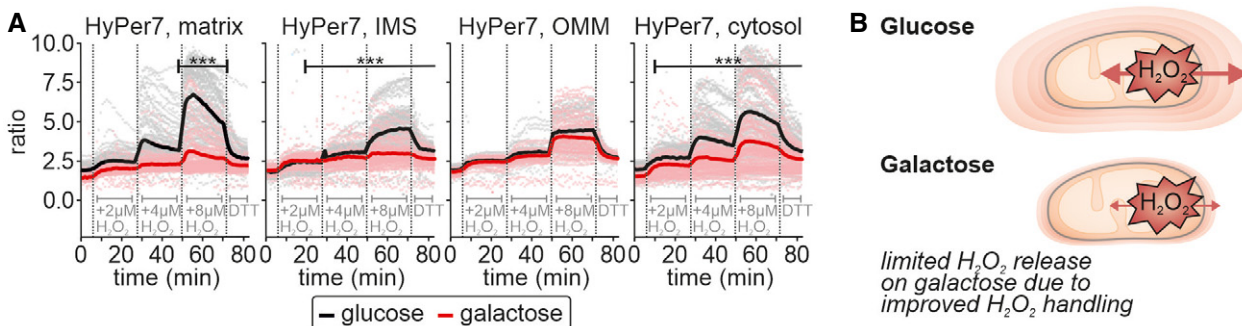


**Figure 4. Growth in the presence of different carbon sources impacts compartmental H<sub>2</sub>O<sub>2</sub> handling.**

- A Response of HyPer7 probes targeted to indicated compartments to treatment with increasing amounts of exogenous H<sub>2</sub>O<sub>2</sub> (2, 4, and 8 μM of H<sub>2</sub>O<sub>2</sub>; 20 mM of DTT). HEK293 cells were grown either with glucose (black curve and data points) or galactose (red curve and data points) as carbon source. The numbers of cells per experiment for each dataset can be found in Appendix Table S6. As most of the data were not normal distributed, instead of a t-test, a Wilcoxon/Mann-Whitney-U-test was performed and samples were compared in pairs. \*\*\*P ≤ 0.001.
- B Model. (Mitochondrial) H<sub>2</sub>O<sub>2</sub> is more efficiently handled in galactose-grown cells in mitochondria and cytosol.

Source data are available online for this figure.

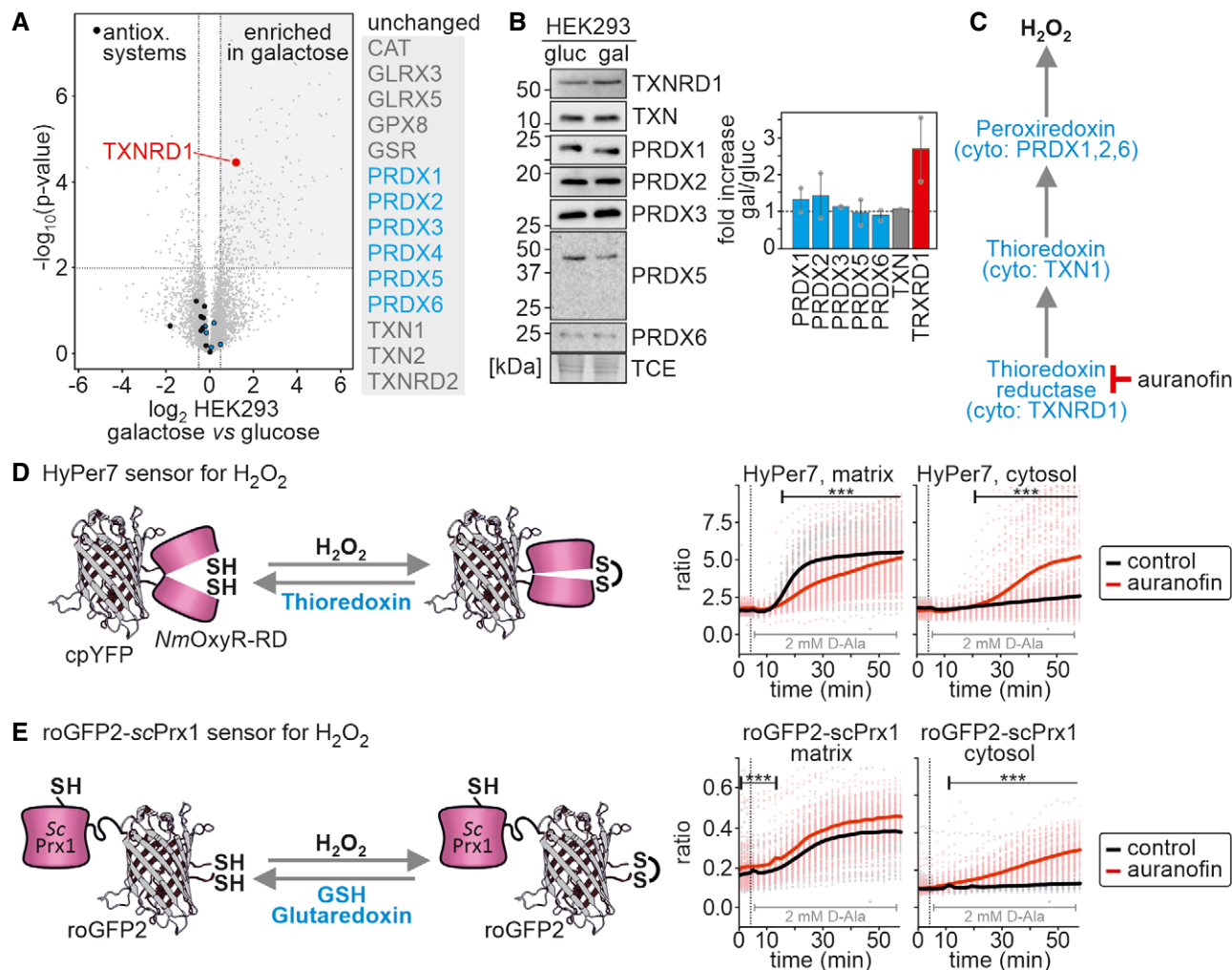


**Figure 5. Increased activity of the cytosolic thioredoxin system limits mitochondrial H<sub>2</sub>O<sub>2</sub> release during increased use of the respiratory chain.**

**A** Protein levels in cells grown on glucose and galactose. Cell lysates were analyzed by quantitative mass spectrometry ( $n = 4$  biological replicates, Dataset EV1). Levels of antioxidative enzymes (especially peroxiredoxins, PRDX in blue) are not changed except for cytosolic thioredoxin reductase (TXNRD1).

**B** Protein levels in cells grown on glucose and galactose. Cell lysates were analyzed by immunoblot ( $n = 2$  biological replicates). Cytosolic thioredoxin reductase (TXNRD1) is increased by more than two-fold in cells grown on galactose compared to glucose-grown cells. The dotted line depicts 1, meaning no change in protein levels.

**C** Mechanisms of H<sub>2</sub>O<sub>2</sub> degradation by peroxiredoxins. Auranofin inhibits thioredoxin reductase and thus the reductive half reaction in the detoxification of H<sub>2</sub>O<sub>2</sub>. Arrows indicate the “flux” of electrons.

**D, E** Response of HyPer7 (D) and roGFP2-scPrx1 (E) probes targeted to indicated compartments to treatment of mtDAO-expressing HEK293 cells with 2 mM of D-Ala (cells generated with the Flp-In T-REX-system). HEK293 cells were incubated either with 1  $\mu$ M of auranofin (red curve and data points) or DMSO (black curve and data points). Solid line represents average, points colored in the lighter version of the respective color are the corresponding ratios measured in individual cells. The numbers of cells per experiment for each dataset can be found in Appendix Table S6. As most of the data were not normal distributed, instead of a t-test, a Wilcoxon/Mann–Whitney-*U*-test was performed and samples were compared in pairs. \*\*\* $P \leq 0.001$ .

Source data are available online for this figure.

induced H<sub>2</sub>O<sub>2</sub> generation (Fig 5D). The thioredoxin system can affect measurements in two ways: first, by attenuating H<sub>2</sub>O<sub>2</sub> levels in the cytosol, for example, by reduction of peroxiredoxin, and second, by accelerating the reducing half reaction of the HyPer7 sensor (Figs 1A and Fig 5D; (Pak *et al*, 2020)). To disentangle these contributions, we employed a different H<sub>2</sub>O<sub>2</sub> sensor, roGFP2-ScPrx1, that we recently developed. Importantly, roGFP2-ScPrx1 is not reduced by the thioredoxin system but by the glutathione system instead (Calabrese *et al*, 2019; Kritsiligkou *et al*, 2021). It comprises

a redox-sensitive green fluorescent protein (roGFP2; Dooley *et al*, 2004) genetically fused with the monothiol Prx1 from *Saccharomyces cerevisiae* (ScPrx1). The ScPrx1 moiety serves to efficiently transfer oxidative equivalents from H<sub>2</sub>O<sub>2</sub> to roGFP2. This probe is predominantly reduced by endogenous GSH/glutaredoxins, which directly reduce the roGFP2 moiety and also ScPrx1 itself. RoGFP2-ScPrx1 oxidation is therefore determined by rapid H<sub>2</sub>O<sub>2</sub>-driven oxidation and slower GSH/glutaredoxin-driven reduction. Oxidation of this probe was also more pronounced upon auranofin treatment

(Fig 5E) indicating that an increase in thioredoxin reductase 1 levels exerts its effect via lowering cytosolic H<sub>2</sub>O<sub>2</sub> levels and to a lesser extent via changes in the efficiency of HyPer7 reduction.

**Increased levels of cytosolic thioredoxin reductase in HeLa cells decrease mitochondrial H<sub>2</sub>O<sub>2</sub> release to the cytosol**

Our data are in apparent contradiction to a recent study with HyPer7 that did not detect mitochondrial H<sub>2</sub>O<sub>2</sub> release to the cytosol upon rotenone treatment and mtDAO-induced H<sub>2</sub>O<sub>2</sub> generation (Mishina et al, 2019; Pak et al, 2020). Based on our data, we hypothesized that this is a consequence of constitutively higher levels of thioredoxin

reductase in HeLa cells compared to HEK293 cells. We confirmed that HeLa cells harbor higher levels of thioredoxin reductase compared to HEK293 cells (Fig 6A; Geiger et al, 2012), and also confirmed that there was no detectable H<sub>2</sub>O<sub>2</sub> release in HeLa cells, despite the fact that matrix HyPer7 becomes oxidized (Fig 6B). Likewise, H<sub>2</sub>O<sub>2</sub> generation by mtDAO provoked cytosolic oxidation of HyPer7 only in HEK293, but not HeLa cells (Fig 6C). We additionally confirmed cell type-specific differences in antimycin A-induced H<sub>2</sub>O<sub>2</sub> release by monitoring HyPer7 responses in COS-7 and 143B cells (Appendix Fig S5). We thereby found that COS-7 cells behaved similarly to HEK293 cells, and in 143B cells like in HeLa cells, we did not detect HyPer7 deflection in the cytosol upon antimycin A treatment.

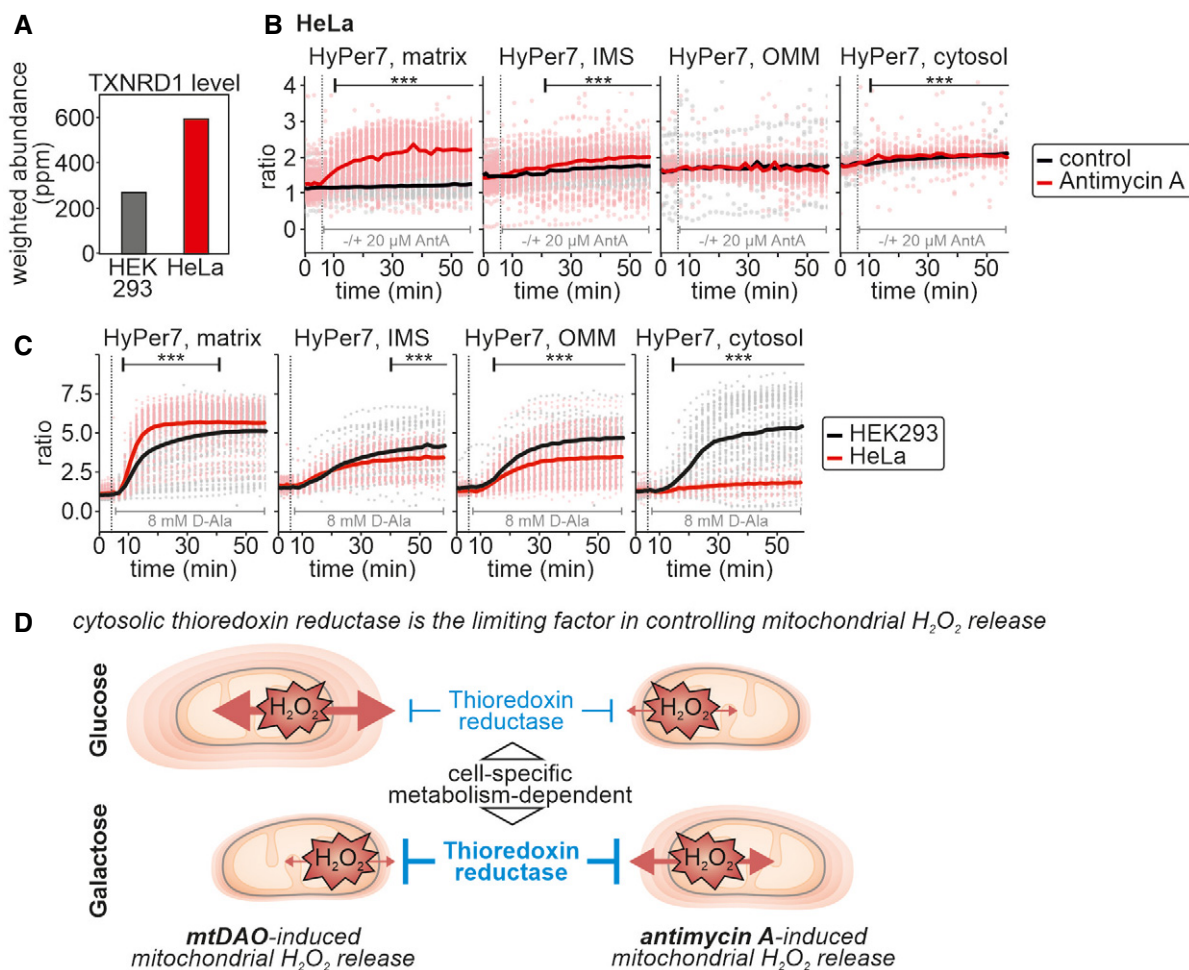


**Figure 6. Increased levels of cytosolic thioredoxin reductase in HeLa cells prevent mitochondrial H<sub>2</sub>O<sub>2</sub> release to the cytosol.**

- A TXNRD1 levels in HeLa and HEK293 cells. Data are from Geiger et al (2012).
- B Response of HyPer7 probes targeted to indicated compartments to incubation with antimycin A (AntA, red curve, and data points) or ethanol as control (black curve and data points). HeLa cells were grown with galactose as carbon source. Solid line represents average, points colored in the lighter version of the respective color are the corresponding ratios measured in individual cells.
- C Response of HyPer7 probes targeted to indicated compartments to treatment of mtDAO-expressing HEK293 (black curve and data points; cell generated with the piggyBAC system) or HeLa (red curve and data points; cell generated with the piggyBAC system) cells with 8 mM of D-Ala. The cells were grown with glucose as carbon source. Solid line represents average, points colored in the lighter version of the respective color are the corresponding ratios measured in individual cells.
- D Model. Cells- and metabolism-specific empowerment of the thioredoxin reductase system controlling H<sub>2</sub>O<sub>2</sub> concentrations following mitochondrial release.

Data information: The numbers of cells per experiment for each dataset can be found in Appendix Table S6. As most of the data were not normal distributed, instead of a t-test, a Wilcoxon/Mann-Whitney-U-test was performed and samples were compared in pairs. \*\*\*P ≤ 0.001. Source data are available online for this figure.

Collectively, our data suggest that cytosolic thioredoxin reductase levels determine whether or not mitochondrial H<sub>2</sub>O<sub>2</sub> can be detected by genetically encoded sensors measuring average H<sub>2</sub>O<sub>2</sub> levels in the bulk cytosol. Furthermore, our data show that thioredoxin reductase levels can change dependent upon metabolic status and cell type and correlate with the level of mitochondrial H<sub>2</sub>O<sub>2</sub> detectable in the cytosol (Fig 6D). However, additionally, as adaptation can also take place on a time scale of minutes, which is insufficient time for significant changes in thioredoxin reductase level we also expect that changes in the flux through different metabolic pathways plays an additional role (Appendix Fig S6).

### Cytosolic peroxiredoxins cooperate in controlling mitochondrial hydrogen peroxide release

Upon growth on galactose, HEK293 cells adapted by increasing the levels of cytosolic thioredoxin reductase. Since, the thioredoxin system drives reduction of peroxiredoxins after they reduced H<sub>2</sub>O<sub>2</sub>, this indicates that the reducing half-reaction during H<sub>2</sub>O<sub>2</sub> detoxification by peroxiredoxins may limit H<sub>2</sub>O<sub>2</sub> handling, rather than the levels of peroxiredoxins. Thus, we next assessed the importance of the cytosolic peroxiredoxins for modulating mitochondrial H<sub>2</sub>O<sub>2</sub> release. To this end, we generated single knockouts of the cytosolic dithiol peroxiredoxins, PRDX1, and PRDX2 using CRISPR-Cas technology (Fig 7A and B). In these cells, when grown on glucose, levels of other antioxidant proteins remained unchanged, in particular the concentrations of the other cytosolic peroxiredoxin (Fig 7A and B). Steady state HyPer7 ratios were also essentially unchanged in both single knockout cell lines (Fig 7C). Mitochondrial production of H<sub>2</sub>O<sub>2</sub> by antimycin A treatment or in cells stably and inducibly expressing mtDAO (in these cells, stable and inducible expression of mtDAO used the piggyBAC system) revealed almost no difference between either peroxiredoxin knockout line as compared to the wild type (Fig 7D and Appendix Fig S7). Only during bolus application of exogenous H<sub>2</sub>O<sub>2</sub>, did HyPer7 in the PRDX1 and PRDX2 knockout cells exhibit an increased oxidation compared to wild-type cells, especially in the matrix and cytosol (Fig 7E). Notably, stable and inducible expression of mtDAO with the piggyBAC system appeared to influence the HyPer7 steady state even in the absence of D-alanine (compare steady state = first 5 min between Fig 7D (mtDAO) and Fig 7E (no mtDAO)).

We did not observe this influence in HEK293 cells stably and inducibly expressing mtDAO using the Flp-In T-Rex system (compare to Fig 3C), and hypothesize that leaky expression in the piggyBAC system contributes to the increased HyPer7 steady state ratio.

Since HyPer7 steady state values were essentially unchanged between compartments and also the reactions to H<sub>2</sub>O<sub>2</sub> were comparably small in the single knockout lines, we wondered whether PRDX1 and PRDX2 complemented for each other in the respective single knockouts. We thus generated a double knockout cell line lacking PRDX1 and PRDX2 (Figs 8A and B). Interestingly, even in this cell line the level of many other antioxidative redox enzymes remained unchanged. Conversely, the HyPer7 steady state ratio differed strongly from the wild type in all compartments assessed including the mitochondrial matrix (Fig 8C, Appendix Fig S1). When we exposed these cells to an external bolus of H<sub>2</sub>O<sub>2</sub>, we observed a strong deflection of HyPer7 in all compartments that appears to be limited by the dynamic range of the HyPer7 sensor (Fig 8D). HyPer7 in double knockout cells containing mtDAO was already at a highly oxidized steady state (without D-alanine addition) especially in the matrix and cytosol. Addition of D-alanine then led only to a minimal deflection because also here the sensor appeared to be limited by its dynamic range (Fig 8E).

Collectively, we demonstrate that cytosolic dithiol peroxiredoxins contribute to cytosolic H<sub>2</sub>O<sub>2</sub> handling in HEK293 cells. They are present in amounts with sufficient reserve capacity so that either PRDX1 and PRDX2 can comfortably complement for the loss of the other enzyme, especially under unperturbed conditions, and that under conditions of increased H<sub>2</sub>O<sub>2</sub> generation increased H<sub>2</sub>O<sub>2</sub> scavenging capacity is mediated not by changes in peroxiredoxin levels but rather by upregulation of the thioredoxin system, mainly thioredoxin reductase (Fig 8F).

## Discussion

Here, using the ultra-sensitive, genetically encoded H<sub>2</sub>O<sub>2</sub> sensor, HyPer7, targeted to different subcellular locations, we investigated the intracellular diffusion of mitochondrial H<sub>2</sub>O<sub>2</sub> in single mammalian tissue culture cells. Our experiments yielded several interesting findings, which include: (i) Peroxiredoxins strongly restrict the intracellular

**Figure 7. Cytosolic peroxiredoxins cooperate in controlling mitochondrial H<sub>2</sub>O<sub>2</sub> release.**

- A, B Peroxiredoxin levels in peroxiredoxin 1 (PRDX1 KO) and peroxiredoxin 2 (PRDX2 KO) knockout cells. The upper subpanel depicts the guides used to generate the KO cell lines. Lysates of the indicated cell lines grown in glucose-containing medium were analyzed by immunoblot (A) and quantitative proteomics (*n* = 4, technical replicates) (B). The right subpanel of B lists the identified proteins belonging to cellular antioxidative systems which are not altered for PRDX1 KO or PRDX2 KO, respectively. In both quantitative proteomics experiments, 4,403 proteins were detected in total.
- C HyPer7 steady state ratios of the indicated cell lines. HyPer7 probes were targeted to the indicated compartments of the respective cell lines. The cells were grown in glucose-containing medium. The numbers of cells per experiment for each dataset can be found in Appendix Table S6. In the boxplot, the central band is the median. The lower and upper hinges correspond to the first and third quartiles. The upper whisker extends from the hinge to the largest value no further than 1.5 times the inter-quartile range, whereas the lower whisker extends from the hinge to the smallest value no further than 1.5 times the inter-quartile range.
- D Response of HyPer7 probes targeted to indicated compartments to treatment of mtDAO-expressing cell lines with 4 mM of D-Ala (black, wild type; red, PRDX1 KO; blue, PRDX2 KO; cell generated with the piggyBAC system). The cells were grown in glucose-containing medium. Solid line represents average, points colored in the lighter version of the respective color are the corresponding ratios measured in individual cells.
- E Response of HyPer7 probes targeted to indicated compartments to treatment with 25 μM of exogenous H<sub>2</sub>O<sub>2</sub>. Indicated cell lines (black, wild type; red, PRDX1 KO; blue, PRDX2 KO) were grown in glucose-containing medium. Solid line represents average, points colored in the lighter version of the respective color are the corresponding ratios measured in individual cells.

Data information: The numbers of cells per experiment for each dataset can be found in Appendix Table S6. As most of the data were not normal distributed, instead of a *t*-test, a Wilcoxon/Mann-Whitney-*U*-test was performed and samples were compared in pairs. \**P* ≤ 0.05, \*\**P* ≤ 0.01, \*\*\**P* ≤ 0.001. Source data are available online for this figure.

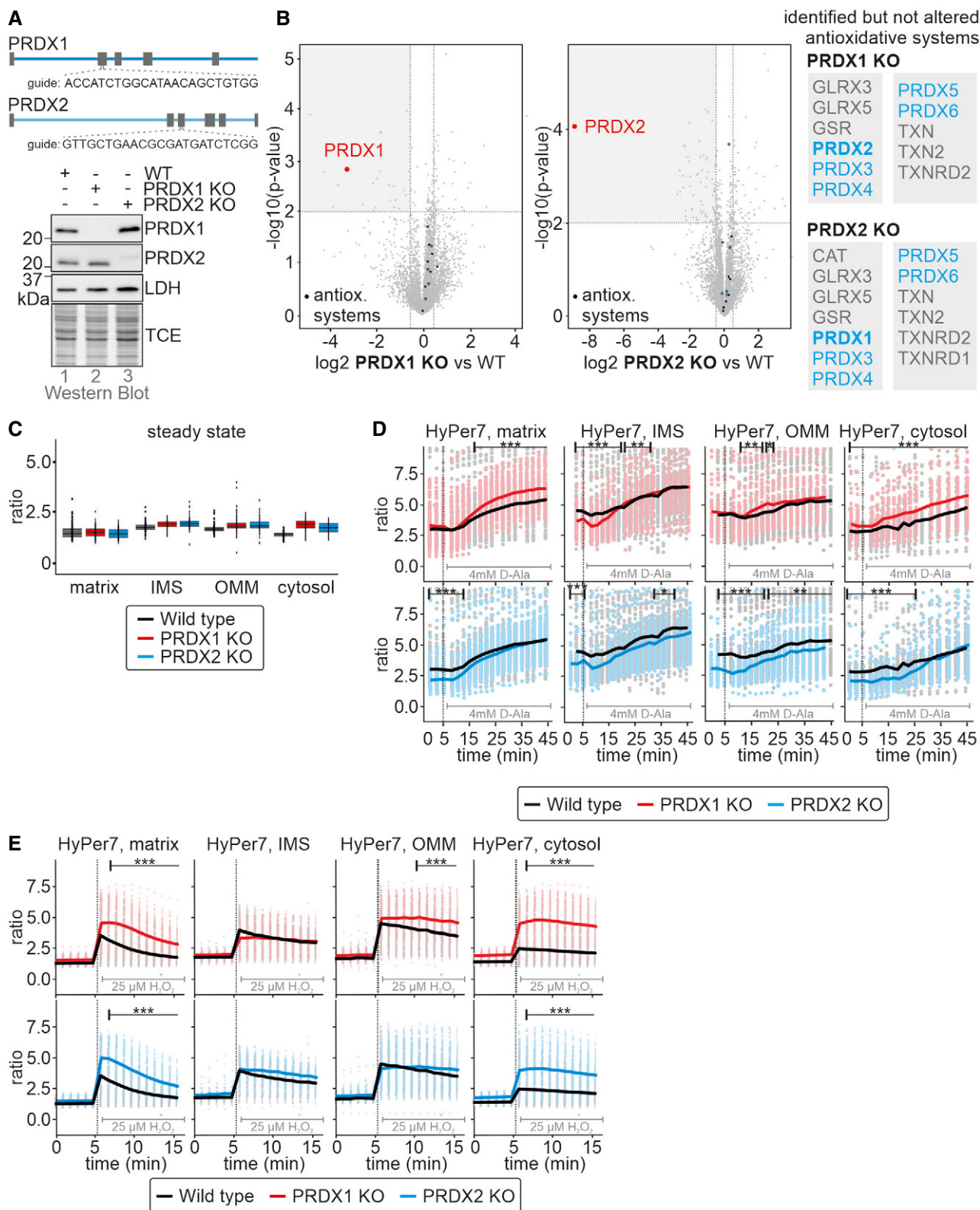


Figure 7.

diffusion of H<sub>2</sub>O<sub>2</sub>. (ii) Peroxiredoxin activity is limited by the availability of thioredoxin reductase, the level of which varies between cell types, explaining previous observations that at first glance seem to be

in contradiction with our findings (Pak *et al*, 2020). (iii) Both H<sub>2</sub>O<sub>2</sub> production and H<sub>2</sub>O<sub>2</sub> removal capacity are modulated by changes in carbon metabolism, that is, glucose versus galactose. (iv)

Mitochondrial H<sub>2</sub>O<sub>2</sub> does not reach the nucleus in detectable quantities, thereby raising important questions regarding proposed models of mitochondrial H<sub>2</sub>O<sub>2</sub> signaling. (v) We observed a high degree of heterogeneity between individual cells in their ability to scavenge H<sub>2</sub>O<sub>2</sub>.

**Cytosolic peroxiredoxins limit amounts of mitochondrial H<sub>2</sub>O<sub>2</sub> in the cytosol**

We observed release of mitochondrial H<sub>2</sub>O<sub>2</sub> using either antimycin A or mtDAO to induce mitochondrial H<sub>2</sub>O<sub>2</sub> production. Using

HyPer7 probes, localized to several different subcellular domains, we were able to show that mitochondrial H<sub>2</sub>O<sub>2</sub> was largely confined to the proximity of mitochondria, as no response of PM or nuclear-localized probes was observed. In HEK293 cells, we observed a small oxidation of the cytosolic HyPer7, which we did not observe in HeLa cells, consistent with previous observations. It is important to reiterate here, that we do not interpret our data as reflecting differences in the release of mitochondrial H<sub>2</sub>O<sub>2</sub> between different cell types, particularly in the mtDAO expression studies. Instead, we believe that the difference reflects different cytosolic H<sub>2</sub>O<sub>2</sub>

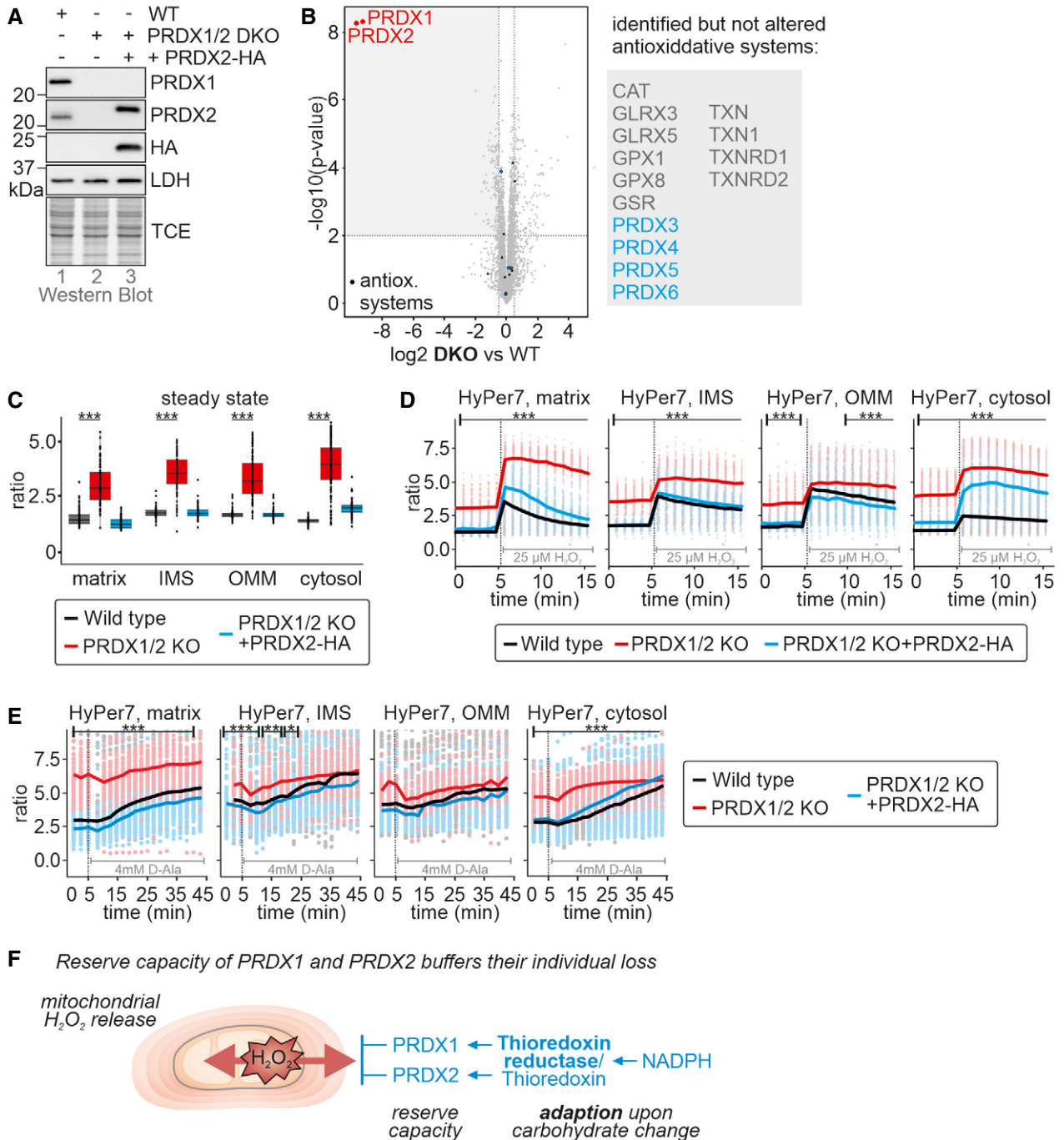


Figure 8.

**Figure 8. Peroxiredoxin 1 and 2 double knockout cells are strongly impaired in handling of mitochondrial H<sub>2</sub>O<sub>2</sub> release.**

- A, B Peroxiredoxin levels in peroxiredoxin 1 and 2 double knockout cells (PRDX1/2 DKO). Lysates of the indicated cell lines grown in glucose-containing medium were analyzed by immunoblot (A) and quantitative proteomics (B). The right subpanel in (B) lists all detected but not altered proteins belonging to cellular antioxidative systems.
- C HyPer7 steady state ratios of the indicated cell lines. HyPer7 probes were targeted to the indicated compartments of the respective cell lines. The cells were grown in glucose-containing medium. The numbers of cells per experiment for each dataset can be found in Appendix Table S6. In the boxplot, the central band is the median. The lower and upper hinges correspond to the first and third quartiles. The upper whisker extends from the hinge to the largest value no further than 1.5 times the inter-quartile range, whereas the lower whisker extends from the hinge to the smallest value no further than 1.5 times the inter-quartile range.
- D Response of HyPer7 probes targeted to indicated compartments to treatment with 25  $\mu$ M of exogenous H<sub>2</sub>O<sub>2</sub>. Indicated cell lines (black, wild type; red, PRDX1/2 DKO) were grown in glucose-containing medium. Solid line represents average, points colored in the lighter version of the respective color are the corresponding ratios measured in individual cells.
- E Response of HyPer7 probes targeted to indicated compartments to treatment of mtDAO-expressing cell lines with 4 mM of D-Ala (black, wild type; red, PRDX1/2 DKO; cell generated with the piggyBAC system). The cells were grown in glucose-containing medium. Solid line represents average, points colored in the lighter version of the respective color are the corresponding ratios measured in individual cells.
- F Model. See discussion for details.

Data information: The numbers of cells per experiment for each dataset can be found in Appendix Table S6. Statistical analysis was only performed to compare the PRDX1/2 DKO with the wild type. As most of the data were not normal distributed, instead of a *t*-test, a Wilcoxon/Mann-Whitney-*U*-test was performed and samples were compared in pairs. \**P*  $\leq$  0.05, \*\**P*  $\leq$  0.01, \*\*\**P*  $\leq$  0.001.

Source data are available online for this figure.

scavenging capacities. The cytosolic HyPer7 probe is freely diffusible in the cytosol and will report on changes in the average H<sub>2</sub>O<sub>2</sub> content of the whole cytosol. In HeLa cells, with very efficient H<sub>2</sub>O<sub>2</sub> scavenging in the cytosol the diffusion of mitochondrial H<sub>2</sub>O<sub>2</sub> will be strongly limited, leading to a steep H<sub>2</sub>O<sub>2</sub> concentration gradient around the mitochondria. Likely, this region of cytosol is simply too small to affect the average cytosolic HyPer7 oxidation. On the contrary, in HEK293 cells, with less efficient cytosolic H<sub>2</sub>O<sub>2</sub> scavenging, mitochondrial H<sub>2</sub>O<sub>2</sub> will diffuse further into the cytosol, the H<sub>2</sub>O<sub>2</sub> concentration gradient surrounding mitochondria will be less steep, the volume of cytosol with increased H<sub>2</sub>O<sub>2</sub> levels will be higher, and the average HyPer7 probe oxidation will give a detectable increase.

We demonstrate that diffusion of mitochondrial H<sub>2</sub>O<sub>2</sub> in the cytosol is regulated by PRDX1 and PRDX2. Both proteins are present in amounts that are high enough to handle much more H<sub>2</sub>O<sub>2</sub> than is normally present in the cell. While deletion of either one of these PRDXs did not induce any compensatory upregulation of the other PRDX in glucose-grown cells, we nonetheless observed that HyPer7 steady state oxidation remained comparable to the wild-type situation. Only upon rapid excess H<sub>2</sub>O<sub>2</sub> generation or exposure did HyPer7 in the PRDX knockout cells become more oxidized than in the wild-type situation. Furthermore, when we deleted both PRDXs together, the HyPer7 steady state became oxidized to an extent that hampered further dynamic analysis of mitochondrial H<sub>2</sub>O<sub>2</sub> release. In summary, there appears to be considerable reserve capacity for H<sub>2</sub>O<sub>2</sub> scavenging in terms of peroxiredoxin availability.

### Thioredoxin reductase availability is an important regulator of cytosolic H<sub>2</sub>O<sub>2</sub> scavenging capacity

Despite the apparent high reserve capacity in terms of peroxiredoxin availability for H<sub>2</sub>O<sub>2</sub> scavenging, we still observed considerable differences between different cell types in terms of H<sub>2</sub>O<sub>2</sub> removal, determined by the ability of H<sub>2</sub>O<sub>2</sub> to diffuse through the cytosol. Intriguingly, the level of thioredoxin reductase appears to be an important limiting factor for H<sub>2</sub>O<sub>2</sub> scavenging. Comparing both HEK293 and HeLa cells and between glucose and galactose grown cells, we observed differences in thioredoxin reductase levels that correlated well with measured differences in H<sub>2</sub>O<sub>2</sub> scavenging. Cells adapted to galactose exhibited increased protein amounts of

cytosolic thioredoxin reductase (but not PRDXs). These cells also demonstrated an improved capacity to handle H<sub>2</sub>O<sub>2</sub> thereby efficiently limiting the amounts of cytosolic H<sub>2</sub>O<sub>2</sub> upon mitochondrial H<sub>2</sub>O<sub>2</sub> generation. Collectively, our data obtained with genetically encoded fluorescent sensors are thereby in line with previous *in vitro* and in cell studies that reported that the thioredoxin system strongly impacts on PRDX activity and H<sub>2</sub>O<sub>2</sub> dynamics in cells (Toppo *et al*, 2009; Portillo-Ledesma *et al*, 2018). Our data also explain seemingly contradictory results in which in HeLa cells no impact of mitochondrial H<sub>2</sub>O<sub>2</sub> release could be detected (Pak *et al*, 2020). In these cells, levels of thioredoxin reductase are higher compared to HEK293 cells essentially abolishing oxidation of cytosolic HyPer7 upon release of mitochondrial H<sub>2</sub>O<sub>2</sub>. Such differences might also explain differences in mitochondrial H<sub>2</sub>O<sub>2</sub> signaling between tissues and during differentiation. It is currently unclear why this should be so, although speculatively it could relate to conservation of NADPH. It is also unclear why peroxiredoxins are apparently present at much higher amounts than is necessary for H<sub>2</sub>O<sub>2</sub> scavenging, although perhaps this relates to their other functions, for example as molecular chaperones (Rhee & Woo, 2020; Troussicot *et al*, 2021). In summary, the rate-limiting step for cytosolic H<sub>2</sub>O<sub>2</sub> handling and thus cytosolic detection of mitochondria-generated H<sub>2</sub>O<sub>2</sub> appears to be in the capacity to reduce PRDXs.

### Implications for mitochondrial H<sub>2</sub>O<sub>2</sub> signaling and its crosstalk with metabolic adaptations

Adaptation of cells to galactose rebalances cellular H<sub>2</sub>O<sub>2</sub> dynamics. On the one hand, it improved H<sub>2</sub>O<sub>2</sub> handling by strengthening the reductive regeneration of PRDXs; on the other hand, it also increased the mitochondrial capacity to generate H<sub>2</sub>O<sub>2</sub>. This led to an unchanged HyPer7 steady state between both carbon sources. However, metabolic adaptations might also offer a temporal window of opportunity for redox signaling as initial flux through the respiratory chain might result in increased generation of H<sub>2</sub>O<sub>2</sub> that is initially not matched by upregulation of antioxidative systems.

Due to the steep gradients of H<sub>2</sub>O<sub>2</sub> around mitochondria, signaling by mitochondrial H<sub>2</sub>O<sub>2</sub> likely takes place in close proximity to mitochondria. Such a confined nature of mitochondrial H<sub>2</sub>O<sub>2</sub> signaling could enable signaling pathways originating from mitochondrial

subpopulations or specific parts of the mitochondrial network within a cell, for example, reflecting intracellular heterogeneities in the mitochondrial network with respect to the membrane potential of respiratory chain activity. Our data also support the use of PRDX-mediated pathways for mitochondrial H<sub>2</sub>O<sub>2</sub> signaling (Sobotta *et al*, 2015; Stocker *et al*, 2018). The detected cytosolic levels of H<sub>2</sub>O<sub>2</sub> upon mitochondrial H<sub>2</sub>O<sub>2</sub> generation are high enough to oxidize HyPer7, and our PRDX knockout data indicate that endogenous PRDXs can efficiently compete with HyPer7 for H<sub>2</sub>O<sub>2</sub>, implying that endogenous PRDXs can efficiently sense the released H<sub>2</sub>O<sub>2</sub>.

In our single cell measurements, we observed substantial intercellular differences in HyPer7 responses. Such heterogeneities are often masked when assessing population averages. We currently can only speculate on their origin, for example that they represent responses of cells at different stages of the cell cycle or cells that maintain different fluxes through pathways providing reducing equivalents for H<sub>2</sub>O<sub>2</sub> detoxification, or cells in which mitochondria exhibit different respiratory chain activities. Using single cell multiplexing approaches to for example, concomitantly assess H<sub>2</sub>O<sub>2</sub> dynamics and cell cycle progression or the mitochondrial membrane potential might in future studies help to mechanistically explain the observed heterogeneities.

## Materials and Methods

### Plasmids and cell lines

For plasmids, cell lines, primers, CRISPR guides, and antibodies used in this study, see Appendix Tables S1–S5. All cell lines were cultivated using Dulbecco's modified Eagle's medium (DMEM) complete containing 4.5 g/l of glucose, 10% fetal bovine serum (FCS), and 500 µg/ml of penicillin/streptomycin at 37°C under 5% CO<sub>2</sub>.

### Generation of Peroxiredoxin knockout cells

Guide RNA sequences targeting human PRDX1 or PRDX2 were cloned into the pSpCas9(BB)-2A-GFP (PX458) vector, which was a gift from Feng Zhang (Addgene plasmid # 48138) (Ran *et al*, 2013). HEK Flp-In™ T-REx™-293 cells were transfected using PEI. After 24 h, FACS sorting was used to collect GFP-positive cells. Single cells were seeded into 96-well plates. Clones were screened using western blot. For complementation, the Flp-In™ T-REx™ system (Invitrogen) was used. For selection of knock-out clones, DMEM complete containing 100 µg/ml of hygromycin and 10 µg/ml of blasticidin was used. Prior to experiments, the expression of stable cell lines was induced for at least 16 h with 1 µg/ml of doxycycline. To express matrix targeted DAO in the PRDX knock-out cell lines, the Su9-DAO construct was cloned into the cumate-inducible PB-CuO-MCS-IRES-GFP-EF1-CymR-Purovector (System Biosciences; PiggyBac system). Knock-out clones were selected with DMEM complete containing 2 µg/ml of puromycin and expression of the cell line was induced with 30 µg/ml of cumate for at least 16 h before the experiment.

### Steady state protein levels

HEK239 MOCK cells grown in glucose or galactose DMEM complete were harvested in 1× Laemmli buffer (2% SDS, 60 mM of Tris-HCl

pH 6.8, 10% glycerol, 0.0025% bromophenol blue), boiled at 96°C for 5 min and subsequently analyzed by SDS-PAGE and western blot. As loading control, 2,2-trichloroethanol (TCE) was added to the SDS gel to visualize protein levels.

### Immunofluorescence

HeLa cells were seeded onto poly-L-lysine coated cover slips in DMEM complete medium. After 24 h, cells were transfected with the respective HyPer7 sensor using PEI (polyethylenimine). After 48 h, cells were fixed using 4% paraformaldehyde for 15 min, blocked with BSA-blocking buffer (10 mM HEPES, 3% BSA, 0.3% triton-X-100) for 1 h and incubated with self-made roGFP2 primary antibody or FLAG antibody for 1 h at RT. Subsequently, incubation with secondary antibody STAR 635P goat anti-rabbit (abberior) or Alexa Fluor 488 goat anti-mouse (invitrogen) for 1 h at RT was followed by conserving the samples with mounting medium (30% glycerol, 12% polyvinyl alcohol, 60 mM of TRIS, 2.5% 1,4-diazabicyclo-2,2,2-octan).

STED microscopy for the HyPer7 localization was performed on a Leica TCS SP8 gSTED 3X system (Leica Microsystems) using a 93× glycerin objective with a numerical aperture of 1.3 (HC PL APO CS2 93×/1.30 GLYC, Leica Microsystems). For gated STED, a pulsed white light laser at 633 nm and a 775-nm STED depletion laser were used. Images were deconvolved using the software Huygens Essential (Scientific Volume Imaging).

### Quantitative label-free proteomics

Cells were seeded in 6-well plates ( $n = 4$ ). After reaching confluence, cells were washed once with PBS, scratched off in 1 ml of PBS and transferred in a 1.5-ml reaction tube. After 5 min of centrifugation at 500 g, supernatant was removed, and lysis buffer was added (4% SDS in PBS containing protease inhibitor). Samples were sonicated 20 times (60 × 60) and boiled at 96°C for 5 min to precipitate proteins, fourfold volume of ice-cold acetone was added, and samples were frozen at –80°C. After thawing, samples were centrifuged for 15 min at 16,000 g, supernatant was removed, and samples were washed twice with 500 µl of ice-cold acetone. The pellet was air-dried. In-solution digest and stage tipping were performed according to the protocols of the proteomics facility from CECAD (<https://www.proteomics-cologne.com/protocols>). All samples were analyzed on a Q Exactive Plus Orbitrap (Thermo Scientific) mass spectrometer that was coupled to an EASY nLC “LC” (Thermo Scientific). Peptides were loaded with solvent A (0.1% formic acid in water) onto an in-house packed analytical column (“containing 2 layers of SDB-RPS disc). Peptides were chromatographically separated at a constant flow rate of 250 nl/min using the following gradient: 3–5% solvent B (0.1% formic acid in 80% acetonitrile) within 1 min, 5–30% solvent B within 91 min, 30–50% solvent B within 17 min, 50–95% solvent B within 1.0 min, followed by washing and column equilibration. The mass spectrometer was operated in data-independent acquisition mode. The MS1 scan was acquired from 400 to 1,220 m/z at a resolution of 140,000. MSMS scans were acquired for 10 DIA windows at a resolution of 35,000. The AGC target was set to 3e6 charges. The default charge state for the MS2 was set to 4. Stepped normalized

collision energy was set to 23.5%, 26%, and 28.5%. The MSMS spectra were acquired in profile mode.

### HyPer7 and roGFP2-Prx1 measurements

Four thousand cells per well were seeded in 100  $\mu$ l of complete DMEM on a poly-L-lysine-coated 96-well plate ( $\mu$ clear, GreinerBio). After 24 h, cells were transfected with plasmids containing sensors using PEI. After 48 h, DMEM was replaced by minimal medium (140 mM of NaCl, 5 mM of KCl, 1 mM of MgCl<sub>2</sub>, 2 mM of CaCl<sub>2</sub>, 20 mM of HEPES, 10 mM of glucose, pH set to 7.4 with NaOH) and the 96-well plate was incubated inside Cytation3 (BioTek) for 40 min at 37°C and 5% CO<sub>2</sub>. For all measurements, a 10 $\times$  in-air microscope and the BioTek LED filter cubes 390  $\pm$  15 nm and 467  $\pm$  15 nm were used. For all measurements, 5 min of steady state were measured after the 40 min “adaptation time”. Two kinds of H<sub>2</sub>O<sub>2</sub> titration were performed. In one, different volumes (20, 40, and 80  $\mu$ l) of a solution with a very low H<sub>2</sub>O<sub>2</sub> concentration were added, each after 20 min, to the same well sequentially, resulting in concentration of  $\sim$  2, 4, and 8  $\mu$ M of H<sub>2</sub>O<sub>2</sub> in the well. Finally, DTT was added as control (50  $\mu$ l, resulting in 20 mM). In the other, 12.5  $\mu$ M of H<sub>2</sub>O<sub>2</sub> were added to single wells and measured for 20 min. DTT was added as control as well. To investigate H<sub>2</sub>O<sub>2</sub> in cell grown in different carbon source, they were grown for at least 1 day in the respective carbon source before conducting the experiment. To investigate to production of H<sub>2</sub>O<sub>2</sub> upon inhibition of the respiratory chain, 30  $\mu$ l of MM containing Antimycine A (20  $\mu$ M f.c.) were added to different wells and measured for 50 min.

For a D-Alanine titration, after 5 min steady state, 30  $\mu$ l of MM containing D- or L-Ala resulting in 1, 2, 4, or 8 mM of D-Alanine or 8 mM of L-Alanine were added to different wells and measured for 50–60 min. To investigate if inhibition of TXNRD1 influence H<sub>2</sub>O<sub>2</sub> dynamics, to HEK293 matrix-DAO cells grown in galactose 2 mM of D- or L-Ala were added combined with or without 1  $\mu$ M of auranofin after 5 min of steady state measurements. Sensor oxidation was followed for 50 min.

For the hypoxia/reoxygenation experiments, cells were prepared as for the other experiments. Ten minutes of steady state were measured at 20% O<sub>2</sub>. Then hypoxia was started and reached 1% O<sub>2</sub> after 30 min. After 200 min at 1% O<sub>2</sub>, reoxygenation was started and 20% O<sub>2</sub> was reached after 1 h. During the whole time, the measurements were conducted every 15 min.

### Data analysis, quantification, and statistical analysis

The acquired images for each experiment were analyzed using the program RRA (“redox ratio analysis,”; Fricker, 2016). With this program, images were aligned, filtered, background-subtracted, and the intensity for both channels as well as the resulting ratio (500/400 or 405/488) was calculated and saved as an excel file. Using R, these excel files were further analyzed, the mean was calculated, figures prepared, and statistics performed. For Cytation3 measurements, the data were first analyzed for normal distribution using a Shapiro–Wilk test. As most of the data were not normally distributed, instead of a t-test, a Wilcoxon/Mann–Whitney-U-test was performed and samples were compared in pairs. Western blot signals were quantified using Image Lab 5.2.1 (Bio-Rad). Error bars represent standard deviation.

## Data availability

This study includes no data deposited in external repositories.

**Expanded View** for this article is available online.

### Acknowledgments

The Deutsche Forschungsgemeinschaft (DFG) funds research in the Laboratory of JR (RI2150/2-2—project number 251546152, RI2150/5-1—project number 435235019, CRC1218 / TP B02—project number 269925409, and RTG2550/1—project number 411422114). VVB was supported by the grant O75-15-2019-1789 from the Ministry of Science and Higher Education of the Russian Federation. The authors thank the CECAD Proteome and Imaging Facilities for the provision of instrumentation, training, and technical support. Open Access funding enabled and organized by Projekt DEAL.

### Author contributions

**Michaela Nicole Hoehne:** Conceptualization; Data curation; Formal analysis; Investigation; Visualization; Writing—original draft; Writing—review and editing. **Lianne J H C Jacobs:** Conceptualization; Data curation; Formal analysis; Investigation; Visualization; Writing—original draft; Writing—review and editing. **Kim Jasmin Lapacz:** Formal analysis; Investigation; Visualization.

**Gaetano Calabrese:** Investigation; Visualization. **Lena Maria Murschall:**

Formal analysis; Investigation; Visualization. **Teresa Marker:** Investigation; Visualization. **Harshita Kaul:** Formal analysis; Investigation. **Aleksandra**

**Trifunovic:** Conceptualization; Supervision. **Bruce Morgan:** Conceptualization; Writing—original draft; Writing—review and editing. **Mark Fricker:** Software; Writing—original draft; Writing—review and editing. **Vsevolod V Belousov:** Resources; Writing—original draft; Writing—review and editing.

**Jan Riemer:** Conceptualization; Formal analysis; Supervision; Funding acquisition; Visualization; Writing—original draft; Project administration; Writing—review and editing.

In addition to the CRediT author contributions listed above, the contributions in detail are:

JR and MNH designed the study and planned experiments. MNH, LJHC, KJL, LMM, TM, and GC performed experiments. JR, LJHC, and MNH analyzed data. MF wrote the RRA software and trained MNH in its use. HK and AT performed and analyzed oxygen consumption experiments and data. VVB provided the HyPer7 plasmid before publication and provided critical input into the planning of the study. BM provided critical input into the planning of the study. JR, BM, VVB, and MNH wrote the manuscript with critical input from all authors.

### Disclosure and competing interests statement

The authors declare that they have no conflict of interest.

## References

- Bienert GP, Moller AL, Kristiansen KA, Schulz A, Moller IM, Schjoerring JK, Jahn TP (2007) Specific aquaporins facilitate the diffusion of hydrogen peroxide across membranes. *J Biol Chem* 282: 1183–1192
- Bleier L, Wittig I, Heide H, Steger M, Brandt U, Drose S (2015) Generator-specific targets of mitochondrial reactive oxygen species. *Free Radic Biol Med* 78: 1–10
- Brand MD (2010) The sites and topology of mitochondrial superoxide production. *Exp Gerontol* 45: 466–472

- Brand MD (2016) Mitochondrial generation of superoxide and hydrogen peroxide as the source of mitochondrial redox signaling. *Free Radic Biol Med* 100: 14–31
- Brand MD (2020) Riding the tiger – physiological and pathological effects of superoxide and hydrogen peroxide generated in the mitochondrial matrix. *Crit Rev Biochem Mol Biol* 55: 592–661
- Calabrese G, Peker E, Amponsah PS, Hoehne MN, Riemer T, Mai M, Bienert GP, Deponte M, Morgan B, Riemer J (2019) Hyperoxidation of mitochondrial peroxiredoxin limits H<sub>2</sub>O<sub>2</sub>-induced cell death in yeast. *EMBO J* 38: e101552
- Calamita G, Ferri D, Gena P, Liquori GE, Cavalier A, Thomas D, Svelto M (2005) The inner mitochondrial membrane has aquaporin-8 water channels and is highly permeable to water. *J Biol Chem* 280: 17149–17153
- Chandel NS (2014) Mitochondria as signaling organelles. *BMC Biol* 12: 34
- Chouchani ET, Pell VR, James AM, Work LM, Saeb-Parsy K, Frezza C, Krieg T, Murphy MP (2016) A unifying mechanism for mitochondrial superoxide production during ischemia-reperfusion injury. *Cell Metab* 23: 254–263
- D'Autreaux B, Toledano MB (2007) ROS as signalling molecules: mechanisms that generate specificity in ROS homeostasis. *Nat Rev Mol Cell Biol* 8: 813–824
- Diebold L, Chandel NS (2016) Mitochondrial ROS regulation of proliferating cells. *Free Radic Biol Med* 100: 86–93
- Dooley CT, Dore TM, Hanson GT, Jackson WC, Remington SJ, Tsien RY (2004) Imaging dynamic redox changes in mammalian cells with green fluorescent protein indicators. *J Biol Chem* 279: 22284–22293
- Drose S, Brandt U (2012) Molecular mechanisms of superoxide production by the mitochondrial respiratory chain. *Adv Exp Med Biol* 748: 145–169
- Fricker MD (2016) Quantitative redox imaging software. *Antioxid Redox Signal* 24: 752–762
- Geiger T, Wehner A, Schaab C, Cox J, Mann M (2012) Comparative proteomic analysis of eleven common cell lines reveals ubiquitous but varying expression of most proteins. *Mol Cell Proteomics* 11: M111.014050
- Goncalves RL, Quinlan CL, Perevoshchikova IV, Hey-Mogensen M, Brand MD (2015) Sites of superoxide and hydrogen peroxide production by muscle mitochondria assessed *ex vivo* under conditions mimicking rest and exercise. *J Biol Chem* 290: 209–227
- Han D, Williams E, Cadenas E (2001) Mitochondrial respiratory chain-dependent generation of superoxide anion and its release into the intermembrane space. *Biochem J* 353: 411–416
- Holmstrom KM, Finkel T (2014) Cellular mechanisms and physiological consequences of redox-dependent signalling. *Nat Rev Mol Cell Biol* 15: 411–421
- Janssen-Heininger YM, Mossman BT, Heintz NH, Forman HJ, Kalyanaraman B, Finkel T, Stamler JS, Rhee SG, van der Vliet A (2008) Redox-based regulation of signal transduction: principles, pitfalls, and promises. *Free Radic Biol Med* 45: 1–17
- Kalinovic S, Oelze M, Kroller-Schon S, Steven S, Vujacic-Mirski K, Kvandova M, Schmal I, Al Zuabi A, Munzel T, Daiber A (2019) Comparison of mitochondrial superoxide detection *ex vivo/in vivo* by mitoSOX HPLC method with classical assays in three different animal models of oxidative stress. *Antioxidants* 8: 514
- Klimova T, Chandel NS (2008) Mitochondrial complex III regulates hypoxic activation of HIF. *Cell Death Differ* 15: 660–666
- Kritsiligkou P, Shen TK, Dick TP (2021) A comparison of Prx- and OxyR-based H<sub>2</sub>O<sub>2</sub> probes expressed in *S. cerevisiae*. *J Biol Chem* 297: 100866
- Liao PC, Franco-Iborra S, Yang Y, Pon LA (2020) Live cell imaging of mitochondrial redox state in mammalian cells and yeast. *Methods Cell Biol* 155: 295–319
- Marchisio MJ, Frances DE, Carnovale CE, Marinelli RA (2012) Mitochondrial aquaporin-8 knockdown in human hepatoma HepG2 cells causes ROS-induced mitochondrial depolarization and loss of viability. *Toxicol Appl Pharmacol* 264: 246–254
- Martin JL, Costa ASH, Gruszczczyk AV, Beach TE, Allen FM, Prag HA, Hinchey EC, Mahbubani K, Hamed M, Tronci L et al (2019) Succinate accumulation drives ischaemia-reperfusion injury during organ transplantation. *Nat Metab* 1: 966–974
- Matlashov ME, Belousov VV, Enikolopov G (2014) How much H<sub>2</sub>O<sub>2</sub> is produced by recombinant D-amino acid oxidase in mammalian cells? *Antioxid Redox Signal* 20: 1039–1044
- McManus MJ, Murphy MP, Franklin JL (2014) Mitochondria-derived reactive oxygen species mediate caspase-dependent and -independent neuronal deaths. *Mol Cell Neurosci* 63: 13–23
- Milev NB, Rhee SG, Reddy AB (2018) Cellular timekeeping: It's redox o'clock. *Cold Spring Harb Perspect Biol* 10: a027698
- Mishina NM, Bogdanova YA, Ermakova YG, Panova AS, Kotova DA, Bilan DS, Steinhorn B, Arner ESJ, Michel T, Belousov VV (2019) Which antioxidant system shapes intracellular H<sub>2</sub>O<sub>2</sub> gradients? *Antioxid Redox Signal* 31: 664–670
- Muller FL, Liu Y, Van Remmen H (2004) Complex III releases superoxide to both sides of the inner mitochondrial membrane. *J Biol Chem* 279: 49064–49073
- Murphy MP (2009) How mitochondria produce reactive oxygen species. *Biochem J* 417: 1–13
- Niemeyer J, Scheuring D, Oestreicher J, Morgan B, Schroda M (2021) Real-time monitoring of subcellular H<sub>2</sub>O<sub>2</sub> distribution in *Chlamydomonas reinhardtii*. *Plant Cell* 33: 2935–2949
- Pak VV, Ezerina D, Lyublinskaya OG, Pedre B, Tyurin-Kuzmin PA, Mishina NM, Thauvin M, Young D, Wahni K, Martínez Gache SA et al (2020) Ultrasensitive genetically encoded indicator for hydrogen peroxide identifies roles for the oxidant in cell migration and mitochondrial function. *Cell Metab* 31: 642–653
- Plecita-Hlavata L, Engstova H, Holendova B, Tauber J, Spacek T, Petraskova L, Kren V, Spackova J, Gotvaldova K, Jezek J et al (2020) Mitochondrial superoxide production decreases on glucose-stimulated insulin secretion in pancreatic beta cells due to decreasing mitochondrial matrix NADH/NAD(+) ratio. *Antioxid Redox Signal* 33: 789–815
- Portillo-Ledesma S, Randall LM, Parsonage D, Dalla Rizza J, Karplus PA, Poole LB, Denicola A, Ferrer-Sueta G (2018) Differential kinetics of two-cysteine peroxiredoxin disulfide formation reveal a novel model for peroxide sensing. *Biochemistry* 57: 3416–3424
- Ran FA, Hsu PD, Wright J, Agarwala V, Scott DA, Zhang F (2013) Genome engineering using the CRISPR-Cas9 system. *Nat Protoc* 8: 2281–2308
- Rhee SG (1999) Redox signaling: hydrogen peroxide as intracellular messenger. *Exp Mol Med* 31: 53–59
- Rhee SG, Woo HA (2020) Multiple functions of 2-Cys peroxiredoxins, I and II, and their regulations via post-translational modifications. *Free Radic Biol Med* 152: 107–115
- Riemer J, Schwarzlander M, Conrad M, Herrmann JM (2015) Thiol switches in mitochondria: operation and physiological relevance. *Biol Chem* 396: 465–482
- Roma LP, Deponte M, Riemer J, Morgan B (2018) Mechanisms and applications of redox-sensitive green fluorescent protein-based hydrogen peroxide probes. *Antioxid Redox Signal* 29: 552–568
- Schieber M, Chandel NS (2014) ROS function in redox signaling and oxidative stress. *Curr Biol* 24: R453–R462
- Sies H, Jones DP (2020) Reactive oxygen species (ROS) as pleiotropic physiological signalling agents. *Nat Rev Mol Cell Biol* 21: 363–383
- Sobotta MC, Liou W, Stocker S, Talwar D, Oehler M, Ruppert T, Scharf AN, Dick TP (2015) Peroxiredoxin-2 and STAT3 form a redox relay for H<sub>2</sub>O<sub>2</sub> signaling. *Nat Chem Biol* 11: 64–70

- Stocker S, Maurer M, Ruppert T, Dick TP (2018) A role for 2-Cys peroxiredoxins in facilitating cytosolic protein thiol oxidation. *Nat Chem Biol* 14: 148–155
- Toppo S, Flohe L, Ursini F, Vanin S, Maiorino M (2009) Catalytic mechanisms and specificities of glutathione peroxidases: variations of a basic scheme. *Biochim Biophys Acta* 1790: 1486–1500
- Troussicot L, Burmann BM, Molin M (2021) Structural determinants of multimerization and dissociation in 2-Cys peroxiredoxin chaperone function. *Structure* 29: 640–654
- Winterbourn CC (2020) Hydrogen peroxide reactivity and specificity in thiol-based cell signalling. *Biochem Soc Trans* 48: 745–754

- Wong HS, Benoit B, Brand MD (2019) Mitochondrial and cytosolic sources of hydrogen peroxide in resting C2C12 myoblasts. *Free Radic Biol Med* 130: 140–150



**License:** This is an open access article under the terms of the Creative Commons Attribution-NonCommercial-NoDeriv 4.0 License, which permits use and distribution in any medium, provided the original work is properly cited, the use is non-commercial and no modifications or adaptations are made.